Article

Detecting and calibrating large biases in global onshore wind power assessment across temporal scales

Chengzhi Hou [1], Zhiwei Xu [1] ✉, Kristopher B. Karnauskas[2,3], Danqing Huang [4] & Huayu Lu [1]

The global capacity for wind power has grown rapidly in recent years, yet uncertainties in wind power density (WPD) assessments still hinder effective climate change mitigation efforts. One major challenge is the significant underestimation of WPD when using coarser temporal resolutions (Δt) of wind speed data. Here, we show that using daily Δt results in an average underestimation of 35.6% in global onshore WPD compared to hourly Δt. This discrepancy arises from the exponential decay of WPD with increasing Δt, reflecting the intrinsic properties of wind speed distributions, particularly in regions with weaker winds. To address this, we propose a calibration method that introduces a correction coefficient to reduce biases and harmonize WPD estimates across temporal resolutions. Applying this method to future wind energy projections under the Shared Socioeconomic Pathway 585 scenario increases global onshore WPD estimates by 25% by 2100, compared to uncorrected daily data. These findings highlight the effectiveness of calibration in reducing uncertainties, enhancing WPD assessments, and facilitating robust policy action toward carbon neutrality.

In recent years, wind power has emerged as a leading renewable energy source for electricity generation, offering significant potential to mitigate climate change by offsetting greenhouse gas emissions[1,2]. Global onshore and offshore wind power installations reached a record 117 Gigawatt (GW) in 2023, according to the Global Wind Energy Council[3]. However, achieving the targets outlined by the United Nations Climate Change Conference and Sustainable Development Goals will still require accelerating this growth to at least 320 GW annually by 2030.

Wind power density (WPD), proportional to the cube of wind speed, is a widely used metric for quantifying the potential wind energy available at a given location[4–6]. It provides a standardized measure for comparing wind resources, independent of turbine size or technical specifications, and serves as the quantitative foundation for wind energy assessments and resource classification[7]. Factors influencing WPD assessments include spatial resolution[8,9], temporal resolution (Δt) of wind data[10,11], and air density[12,13]. Among these, temporal resolution has a particularly pronounced effect due to the cubic relationship between wind speed and WPD[14]. High-speed wind events, characterized by short-term variability and disproportionately large contributions to WPD, are often smoothed or lost with coarser Δt data[15]. This leads to substantial underestimations in wind power calculations and related environmental impact assessments[10]. For example, monthly averaged wind speeds have been shown to underestimate total wind power by up to 48% compared to hourly measurements from a wind tower in Boulder, CO, USA[16]. Similarly, daily wind speed data from the fifth-generation atmospheric reanalysis of the global climate produced by the European Centre for Medium-Range Weather Forecasts (ERA5) underestimates global offshore wind power by 10–30% relative to hourly estimates[17].

[1]School of Geography and Ocean Science, Nanjing University, Nanjing, China. [2]Department of Atmospheric and Oceanic Sciences, University of Colorado, Boulder, CO, USA. [3]Cooperative Institute for Research in the Environmental Sciences, University of Colorado, Boulder, CO, USA. [4]School of Atmospheric Sciences, Nanjing University, Nanjing, China. ✉e-mail: zhiweixu@nju.edu.cn

High-resolution data are therefore critical to accurately capturing wind speed variability and improving WPD estimates. However, such data are often challenging to obtain and computationally demanding to process[11]. Practical applications in global and regional wind power assessments often rely on coarser Δt data (Supplementary Table 1), such as daily or even monthly averages, due to accessibility and resource constraints[18,19]. Early global wind power assessments, for instance, employed 6-hour or daily wind speed data[20,21], while analyses of historical changes in wind energy potential often depend on archived low-resolution data. State-of-the-art global climate models (GCMs) in the Coupled Model Intercomparison Project Phase 6 (CMIP6) typically provide daily wind speed data, exacerbating uncertainties in WPD projections[16,22].

Addressing these challenges requires a systematic evaluation of Δt-induced bias, allowing us to balance the trade-offs between accuracy and practical efficiency. To develop robust calibration methods to harmonize WPD estimates across resolutions is also critical but remains unresolved[10,16]. Furthermore, most research has focused on regional analyses[17], leaving the global implications—essential for international policy frameworks—largely underexplored. If a robust relationship between WPD and Δt exists, it would be possible to correct the bias and yield accurate WPD estimates even with coarser Δt, reducing computational demands.

This study investigates the impact of Δt on WPD calculations at a global scale using wind speed data from multiple sources, including high-resolution observations (Supplementary Fig. 1), climate reanalyses (ERA5, and reanalysis datasets from the National Centers for Environmental Prediction/National Centers for Atmospheric Research (NCEP/NCAR) and the NCEP-US Department of Energy (NCEP-DOE)), and climate model simulations from CMIP6. A robust statistical relationship between WPD and Δt is identified, providing a foundation for a calibration method to standardize WPD estimates across temporal resolutions. This approach offers a practical solution for reducing uncertainties in WPD assessments, facilitating wind energy resource planning, and informing policymaking for sustainable energy development.

Results

Underestimation of WPD using coarse temporal resolutions

To demonstrate the effects of temporal resolution on wind speed variability and WPD estimates, a rural station in southern Canada (52.3°N, 111.8°W) was chosen from stations with high-resolution wind speed observational data, ensuring representation of diverse wind conditions. Hourly observational data at this site during May 2021 capture frequent fluctuations and wind gusts exceeding 15 m s^{-1}, with a standard deviation of 3.9 m s^{-1} (Supplementary Fig. 2a). In contrast, daily data smooth these variations, reducing the standard deviation to 2.9 m s^{-1} and diminishing the frequency and magnitude of strong gusts. Similar patterns are observed in ERA5 reanalysis data at the same location, where standard deviations decrease from 3.2 m s^{-1} (1-hour) to 2.6 m s^{-1} (daily) (Supplementary Fig. 2b). This smoothing effect of coarse Δt eliminates high-frequency variability and suppresses the upper percentiles of wind speeds, which dominate WPD calculations. Consequently, WPD estimates are underestimated by 24.5% (observations) and 18.3% (ERA5 reanalysis) at this site.

Globally, observational data reveal consistent spatial patterns for WPD(daily) and WPD(1-hour) (Fig. 1a, b), both aligning well with prior global wind power assessments[16,20,21]. However, coarse Δt introduces substantial underestimation. On average, WPD(daily) underestimates WPD(1-hour) by 35.6%, with relative biases ranging from 20–40% at most sites (Fig. 1c). Spatial variations are evident: high-WPD regions (e.g., northern Europe, central USA, central Asia, and southwestern Australia) exhibit low biases, while low-WPD regions (e.g., southern Europe, eastern USA, Brazil, the Middle East, East Asia, and northern Australia) can experience biases of up to 60% (Fig. 1c).

ERA5 reanalysis similarly highlights distinctive regional patterns (Fig. 1d, e) consistent with observations. Mid- to high-latitude regions and subtropical deserts exhibit relatively high WPD (>200 W m^{-2}), whereas tropical regions generally have low WPD (<50 W m^{-2}). However, ERA5 reinforces the underestimation trend with daily data (Fig. 1f). Similar findings are evident in both NCEP/NCAR and NCEP-DOE reanalysis datasets (Supplementary Fig. 3). Across global terrestrial areas, the average WPD bias between hourly and daily ERA5 data is approximately 20%, with biases exceeding 60% in tropical and mountainous regions where wind speeds are generally low. These consistent patterns across observations and reanalyses underscore that Δt effects are less (more) pronounced in strong (weak) wind environments.

Moreover, Δt significantly affects actual electrical power production (AEP) calculations. Using a General Electric GE 1.5 s wind turbine as an example (Supplementary Fig. 4), AEP estimates derived from daily wind speed data differ markedly from those based on hourly data (Supplementary Fig. 5), emphasizing the critical role of temporal resolution in accurately evaluating wind energy potential.

Intrinsic dependence of WPD decay on temporal resolutions

To explore why WPD calculations differ across wind speed data with varying Δt, we analyzed the statistical characteristics of their distributions. Using the rural station in southern Canada as an example, the wind speed data were fitted to a Weibull probability density function (PDF). Though the Weibull PDF has been shown to give a good fit to observed wind speed distributions in most cases[10], here it was used solely for fitting the distribution, while WPD calculations were performed using the statistical method described in the Methods section.

In this case, the Weibull distribution provides a good fit for the hourly wind speed series, with a shape parameter $k = 1.93$ and a scale parameter $c = 6.53$ (Fig. 2a). However, as Δt coarsens, the wind speed distribution becomes increasingly constricted, with a notable shortening of the tail representing high wind speeds. This results in an increase in k and a decrease in c, shifting the distribution toward a more normal shape. Notably, wind speed data with daily or coarser Δt cannot be accurately represented by the Weibull distribution, as k exceeds the theoretical threshold of 3.042[23].

This shift in the wind speed distribution due to coarser Δt directly impacts WPD calculations. To quantify this, we calculated WPD across different Δt values using global observations. As illustrated by four representative sites in Figs. 2b, c, the relationship between WPD and Δt follows an exponential function as Eq. (1)

$$WPD\,(\Delta t) = a \exp(-b\Delta t) \tag{1}$$

Here, a represents the theoretical maximum WPD (WPD$_{max}$) associated with the finest Δt, and b quantifies the rate of WPD decline with increasing Δt. Larger b values indicate a more rapid reduction in WPD with coarser Δt (Fig. 2b). The fitting results indicate that a 6-hour Δt reduces WPD to approximately 80–90% of WPD$_{max}$, whereas daily averaging can lower it to as little as 55% of WPD$_{max}$ in certain cases (Fig. 2c). Moreover, although WPD$_{max}$ (equal to a) may be slightly lower than the WPD calculated from finer Δt values (e.g., 1-hour or even higher resolutions), a exhibits a strong positive correlation with WPD(1-hour) (Fig. 2d), indicating that WPD(1-hour) is a reasonable approximation of a, the theoretical maximum WPD.

Unlike the stretched exponential model proposed by a previous study[10], our exponential function reveals significant negative correlations between a and b, and between b and WPD(1-hour). As shown in Fig. 2e, f, regions with smaller a and lower WPD(1-hour) exhibit larger b values, indicating a steeper WPD decline with coarser Δt. Conversely, in regions with higher a and WPD(1-hour), the decline is less pronounced. These results align with previous findings[17] and confirm that WPD

underestimation due to coarse Δt is more pronounced in regions with lower wind power potential. Indeed, the ratio of WPD(Δt) to WPD(1-hour) diminishes exponentially as Δt increases, with the decline rate being steeper for lower WPD(1-hour), as shown by site 4 with the smallest a (Fig. 2c).

Globally, the spatial distribution of parameters a and b highlights distinct regional patterns (Fig. 2g, h), and most sites (>95.8%) exhibit robust exponential fits, with coefficients of determination (R^2) exceeding 0.7 (Fig. 2i). Regions with higher a—indicative of strong wind speeds and high wind power potential—include northern Europe, central USA, central Asia, southwestern Australia, southern South America, and some coastal areas. These regions typically have lower b values (<0.01), indicating minimal WPD decline with coarser Δt. Conversely, regions with lower a, such as southern Europe, eastern USA, Brazil, the Middle East, and East Asia, exhibit higher b values, suggesting that WPD calculations in these areas are more sensitive to coarse Δt.

Finally, the decay relationship between WPD and Δt is evident not only in observational data but also in ERA5 reanalysis (Supplementary Fig. 6), demonstrating that Δt effect on WPD calculations is independent of data source. The strong correlation between parameters a and b suggests that this effect is likely an intrinsic property of the wind speed distribution itself, rather than a site-specific attribute. The parameter b, which governs the exponential decay of WPD with respect to Δt, is intrinsically linked to general wind-energy conditions represented by parameter a.

Calibration of WPD bias across temporal scales

The robust relationship between parameters a and b indicates that sites with distinct a values—derivable from WPD(1-hour)—exhibit varying decay characteristics, providing a foundation for rectifying WPD estimates derived from coarser Δt. To address this, we propose a calibration coefficient, $K(\Delta t\text{-1hour})$, which quantifies the relative bias between WPD(Δt) and WPD(1-hour). This coefficient enables the alignment of WPD estimates from varying Δt values to WPD(1-hour). Details of $K(\Delta t\text{-1hour})$ definition, calculation, and the rationale for using WPD(1-hour) as the "target" for rectification are provided in the Methods section.

The global distribution of $K(\text{daily-1hour})$ based on observations (Fig. 3a) shows that regions with lower K values generally correspond
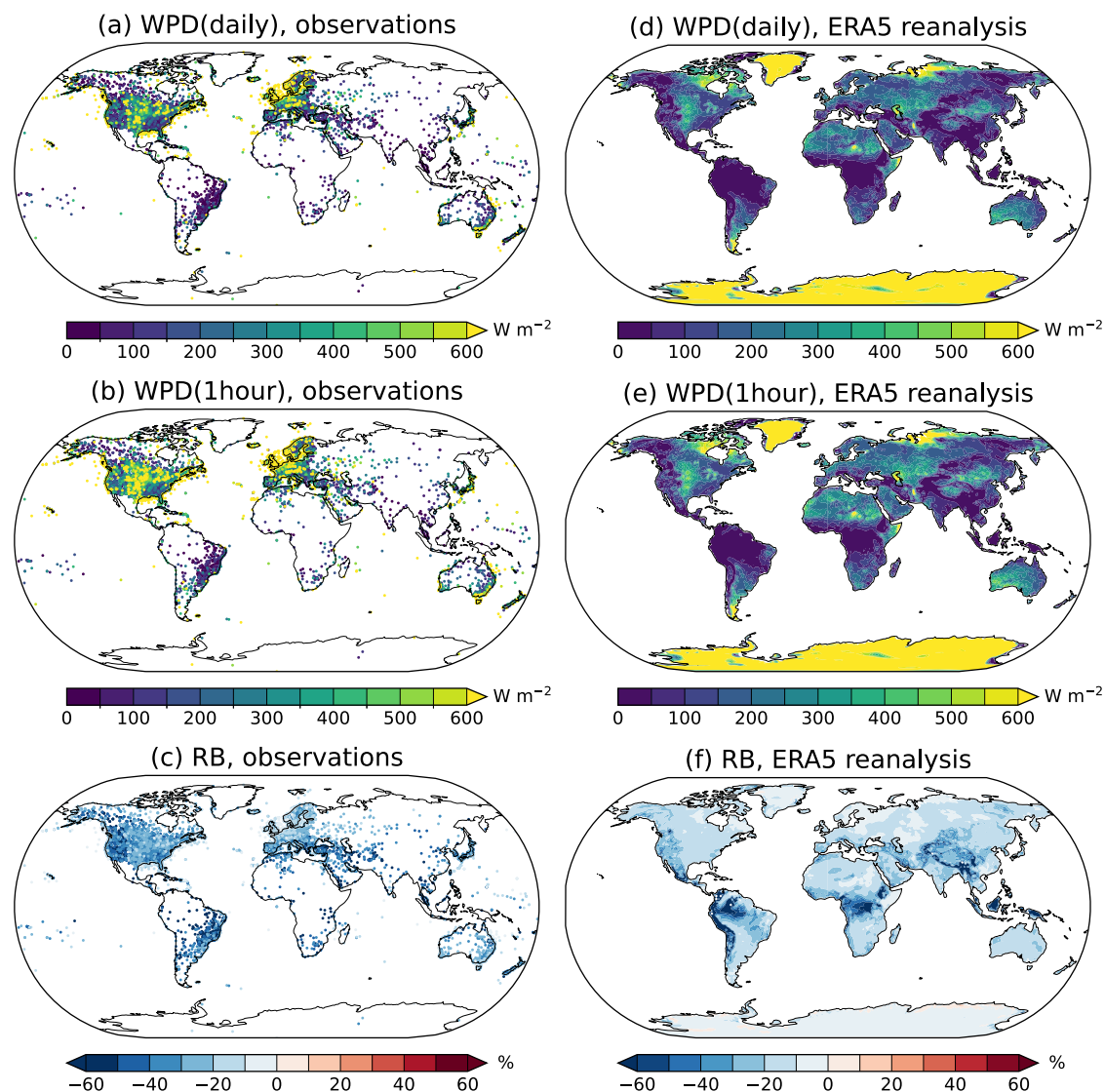

Fig. 1 | Global wind power density (WPD) at 100 m hub height from observations and climate reanalysis with different temporal resolutions (1973–2021). The maps show global WPD distribution derived from observational data at daily (**a**) and hourly (**b**) resolutions, along with their relative bias (RB, %) (**c**). Similarly, WPD distributions from the fifth-generation European Centre for Medium-Range Weather Forecasts (ECMWF) atmospheric reanalysis (ERA5) using daily (**d**) and hourly (**e**) resolutions are shown, with their corresponding relative bias (RB, %) (**f**). Source data are provided as a Source Data file.
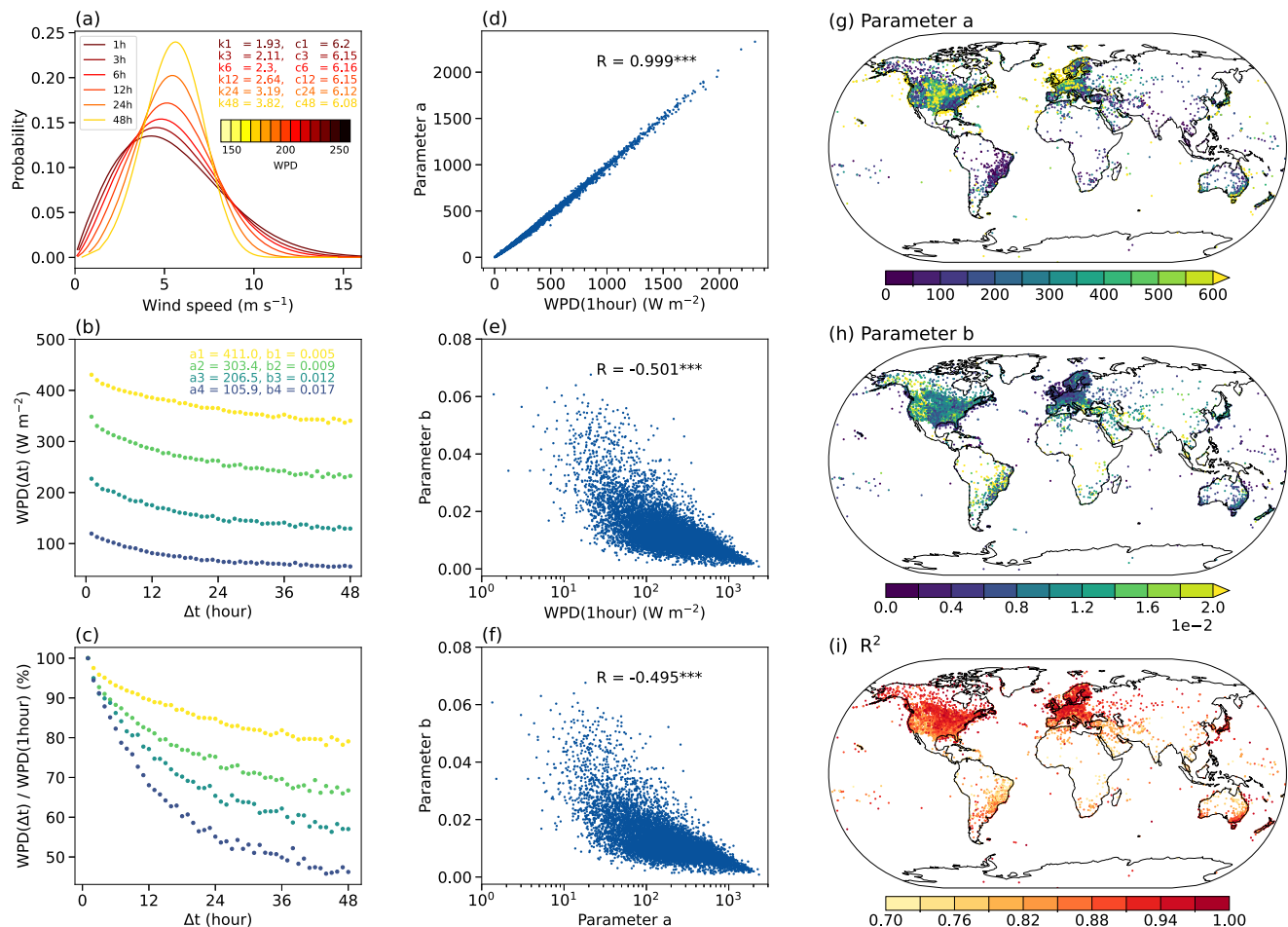
Fig. 2 | Relationship between wind power density (WPD) and temporal resolutions (Δt). a Wind speed distribution for different Δt values (1-hour to 48-hour) fitted with Weibull probability density function, using wind speed observational data (2014–2021) from a rural station in southern Canada (52.3°N, 111.8°W; same site as Supplementary Fig. 2). Parameters k and c describe the Weibull shape and scale, respectively, and the numbers in the panel following k and c (e.g., 1, 3, 6, ...) indicate the corresponding Δt values (e.g., 1-hour, 3-hour, 6-hour, ...). WPD for this example was calculated based on the statistical method according to Eq. (5). **b** Exponential fits of WPD versus Δt for four global sites representing different WPD levels: Site 1 (southeast Australia, 38.4°S, 141.6°E, WPD: ~400 W m^{-2}), Site 2 (Kazakhstan, 49.6°N, 73.3°E, WPD: ~300 W m^{-2}), Site 3 (southern Canada, 51.7°N, 112.7°W, WPD: ~200 W m^{-2}), and Site 4 (southern USA, 35.4°N, 94.8°W, WPD: ~100 W m^{-2}). Each site's fitted curve is shown in a different color. Parameters a and b for each site are labeled as $a1$, $a2$, $a3$, $a4$

and $b1$, $b2$, $b3$, $b4$, respectively. **c** Ratio of WPD(Δt) to WPD(1-hour) as a function of Δt, corresponding to the sites in panel (b). Each site's fitted curve is color-matched with (**b**). **d** Scatter plot of WPD(1-hour) versus parameter a, with *** denoting a correlation exceeding the 99.9% significance level in *t*-test. **e** Scatter plot of WPD(1-hour) versus parameter b. **f** Scatter plot of parameter a versus b. **g** Global distribution of parameter a. **h** Global distribution of parameter b. **i** Global distribution of the coefficient of determination (R^2) for the exponential fits of WPD versus Δt. Sites with $R^2 < 0.7$ (accounting for less than 4.2% of all sites), which show abnormal WPD values and negative b values likely due to data anomalies, were excluded from the analysis. The fitting was performed using 1-hour resolution wind speed data and Eq. (1), with parameters a and b determined for each site. Source data are provided as a Source Data file.

with high wind-energy areas, such as northern Europe, central Asia, central USA, southwestern Australia, southern South America, and certain coastal zones. In contrast, higher K values—indicating significant discrepancies between WPD(daily) and WPD(1-hour) —are observed in relatively flat inland terrains such as East Asia, southern Europe, eastern USA, and Brazil, where wind power generation is already widely implemented. Furthermore, K(daily-1hour) derived from ERA5 reanalysis (Fig. 3b) aligns well with observations, supporting the applicability of the calibration approach across diverse datasets.

Statistical analysis reveals a moderate but significant negative correlation between WPD(daily) and K(daily-1hour) ($R = -0.49$, $p < 0.001$; Fig. 3c). Regions with lower WPD(daily) exhibit higher K values; for instance, K can reach 5.0 when WPD(daily) falls below 10 W m^{-2}, while K approximates 1.5 when WPD(daily) exceeds 400 W m^{-2}. As most sites fall within the WPD(daily) range of 10 and 400 W m^{-2} (Fig. 1a), calibrations using K values of 1.5–2 are particularly relevant. Interestingly, sites with WPD(daily) exceeding about

1000 W m^{-2} have K values below 1.0 (Fig. 3c), consistent with the positive relative bias in Fig. 1c. This phenomenon is actually attributed to deceptive high-speed wind events arising from averaging wind speeds above the cut-out threshold (Supplementary Fig. 7), which are unsuitable for electricity production.

To facilitate practical use, K values were categorized by WPD levels (Fig. 3d). For WPD Level I (0–50 W m^{-2}), the median K value is 2.12, albeit with substantial variation, while for WPD Level VI (>400 W m^{-2}), the median K value is 1.21, with much narrower variability. These categorized K values can be directly used to adjust WPD across different grades. Additionally, a global gridded dataset of K values at 1° × 1° resolution was generated (Supplementary Fig. 8). This dataset preserves large-scale spatial features, enabling straightforward correction of WPD at specific locations with present conditions by referencing the nearest grid point's K value.

Calibration coefficients K(Δt-1hour) were also derived for 6-hour and 3-hour resolutions, commonly used in previous studies
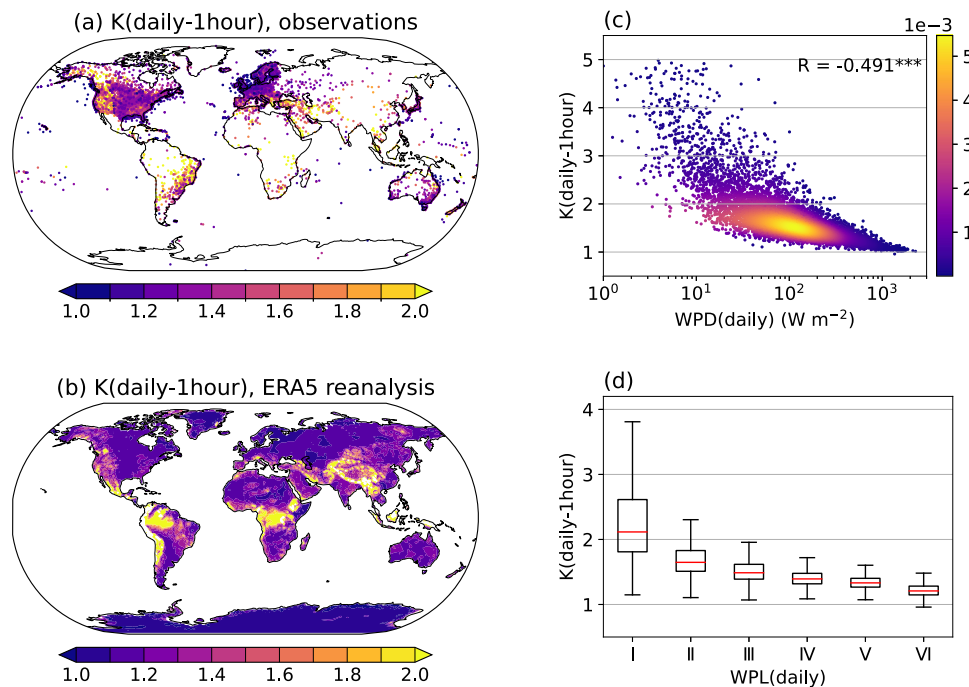
Fig. 3 | Calibration coefficient K(daily−1hour) derived from observational data and climate reanalysis. a Global distribution of K(daily−1hour) derived from observational data spanning 1973–2021. **b** Global distribution of K(daily−1hour) calculated from the fifth-generation European Centre for Medium-Range Weather Forecasts (ECMWF) atmospheric reanalysis (ERA5) for the same period. **c** Scatter plots of wind power density (WPD, daily) versus K(daily−1hour) based on observations. The color bar represents point density, computed in linear WPD space but displayed on a logarithmic x-axis for clarity. *** denotes statistical significance at the 99.9% confidence level (*t*-test). **d** Boxplots of K(daily−1hour) categorized by WPD levels (WPL, I–VI), as defined by the National Renewable Energy Laboratory[7]. Levels I–VI correspond to WPD ranges of 0–50, 50–100, 100–200, 200–300, 300–400, and >400 W m⁻², respectively, based on observational data. Median K values are indicated by red lines within each box. Outliers (K(daily-1hour)>5.0, accounting for less than 1.9% of total sites) were excluded from the analysis due to anomalously low WPD values, likely resulting from data anomalies. Data for the boxplots are provided in Supplementary Table 3. Source data are provided as a Source Data file.

(Supplementary Table 1). As shown in Supplementary Fig. 9, the relationship between WPD and K at these resolutions mirrors that of daily Δt, with slightly lower K values. Applying the same methodology, WPD and K values were calculated from ERA5, NCEP/NCAR, and NCEP-DOE reanalysis datasets across various Δt values (Supplementary Fig. 10). In all cases, K maintained a significant negative correlation with WPD, reinforcing the robustness of the calibration method (Supplementary Fig. 11).

Taken together, these findings suggest that the statistical relationship between K and WPD, derived from diverse datasets, can effectively rectify WPD estimates across different Δt ranges. This calibration approach not only aligns WPD(daily) with WPD(1-hour) but also extends to WPD(3-hour) where applicable, offering a practical solution for harmonizing global wind power assessments and minimizing uncertainties in policy-relevant decisions.

Implications for future wind power assessment

To illustrate the uncertainties in assessing future wind power potential using coarse-resolution wind speed data, and to demonstrate the utility of the proposed calibration coefficient K, we provide an example based on the Earth system model (EC-Earth3) from CMIP6. The global distribution of WPD derived from daily wind speed data in the EC-Earth3 model under the Shared Socioeconomic Pathway 585 (SSP585) scenario for 2100 (Fig. 4a) shows spatial patterns similar to those observed during the historical period in ERA5 (Fig. 1d). According to the model, the average global onshore WPD(daily) is projected to be approximately 120 W m⁻² by 2100 (SSP585 scenario; Fig. 4g). However, analysis of 3-hour wind speed data reveals a substantial underestimation when comparing WPD(daily) with WPD(3-hour) (Fig. 4d), despite similar spatial distributions. This discrepancy results in an

average deviation of -30.7% for future WPD across global land (Fig. 4f), aligning closely with the -35.6% bias observed historically in the observational data (Fig. 1c). Regions such as East Asia, southern Europe, and USA−where wind power generation is extensively implemented−exhibit particularly pronounced biases.

Applying the calibration coefficient K(daily-3hour) significantly improves WPD estimates (Fig. 4b). The calibrated WPD(3-hour) reduces the relative bias between WPD(3-hour) and WPD(daily) (Fig. 4e), decreasing the average deviation from −30.7% to −15.0% (Fig. 4f). By applying K(daily-1hour), the global average onshore WPD increases to >150 W m⁻², representing a 25% enhancement relative to daily data (120 W m⁻², Fig. 4g).

These results emphasize the practicality of calibrating WPD using K in scenarios where high-resolution wind speed data are unavailable. This calibration method is especially valuable given that publicly accessible CMIP6 model outputs typically offer wind speed data at resolutions no finer than 3 hours, with most models providing only daily data[11]. The simplicity of the K-based approach enables accurate assessments without requiring computationally intensive high-resolution data, making it particularly advantageous in resource-constrained settings.

It is important to note that this study focuses on the impact of Δt on absolute future global onshore WPD rather than changes relative to the present. As shown in Supplementary Fig. 12, the CMIP6 multi-model mean indicates statistically insignificant decreasing trends in global onshore WPD over the period 2015–2100. Furthermore, the relative changes in WPD remain largely unaffected by the application of K across different greenhouse gas emission scenarios. It may imply that Δt has a minimal impact on WPD trend estimation, whether for historical periods (Supplementary Fig. 13) or future projections
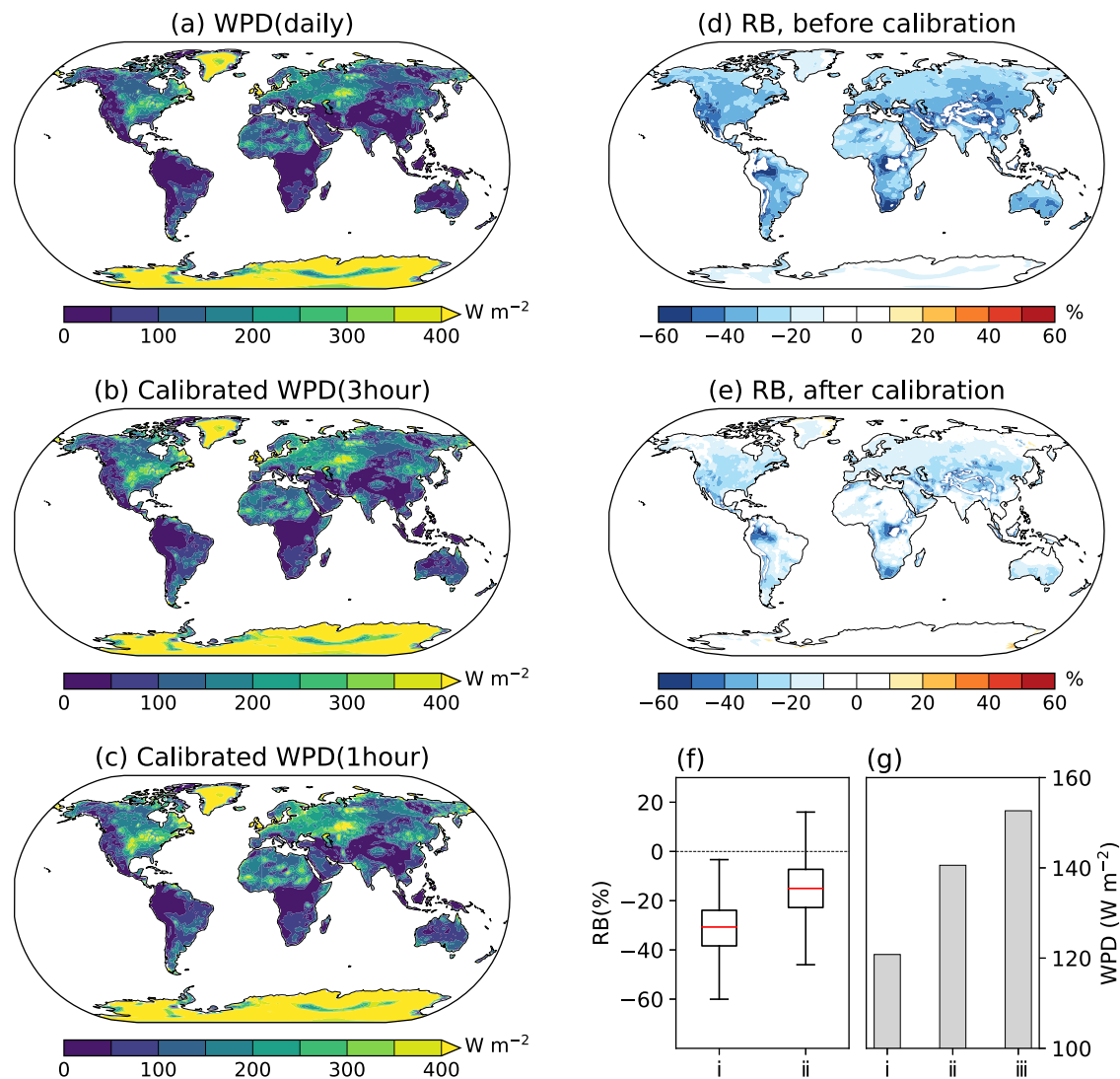
Fig. 4 | Projected global wind power density (WPD) distribution at the hub height (100 m) under the Shared Socioeconomic Pathway 585 scenario for 2090–2100, based on the Earth system model (EC-Earth3) simulations. a Global WPD(daily) derived from daily wind speed data. **b** Calibrated WPD(3-hour), calculated using WPD(daily) and K(daily-3hour). **c** Calibrated WPD(1-hour), calculated using WPD(daily) and K(daily-1hour). **d** Relative bias (RB) between WPD(daily) and WPD(3-hour), based on daily and 3-hour wind speed data from the climate model. **e** Relative bias (RB) between calibrated WPD(3-hour) and original WPD(3-hour). The calibrated WPD(3-hour) was calculated using WPD(daily) and K(daily-3hour). **f** Boxplots of RB for (i) WPD(daily) versus WPD(3-hour), and (ii) calibrated WPD(3-hour) versus original WPD(3-hour). **g** Bar chart showing average global onshore WPD for different temporal resolutions and calibrations: (i) WPD(daily), (ii) calibrated WPD(3-hour), and (iii) calibrated WPD(1-hour). Antarctica is excluded from the analysis due to its current unsuitability for wind power development. Source data are provided as a Source Data file.

(Supplementary Fig. 12; Supplementary Note 1). While uncertainties persist in GCMs regarding wind speed projections, including discrepancies in simulated magnitude and trends[16,22], one certainty is that using daily data to compute wind energy resources consistently results in at least a 30% negative bias on global onshore WPD. Consequently, while calibration may not critically affect assessments of relative changes in WPD—provided both historical and future simulations share consistent biases—it is indispensable for minimizing errors in absolute WPD estimates.

Discussion

Our study reveals substantial biases in WPD estimates when using wind speed data with coarse Δt. These biases intensify as Δt increases, particularly in low-wind regions, leading to significant underestimations in WPD. Importantly, the decay in WPD with Δt is independent of data sources, as consistent patterns are observed across observational data and multiple reanalysis products (Fig. 2, Supplementary Figs. 3, 6). This

phenomenon is driven by the intrinsic characteristics of wind speed distributions: high-speed wind events, which dominate the upper percentiles, often occur over shorter timescales. For example, the strongest phase of a synoptic-scale extratropical cyclone often spans an hour to a day[24]. When measurement intervals are too long, or when time series are averaged over extended Δt intervals (e.g., daily)[25], peak wind speeds are smoothed out. Because of the cubic relationship between wind speed and turbine power output[26], these omissions amplify underestimations in WPD and actual energy production.

While wind speed time series generally follow a Weibull distribution[10,27], this model becomes inadequate when the number of independent observations is insufficient[23,28]. Our findings indicate that as Δt coarsens from 1-hour to daily—reducing observations from 8,760 to 365 per year—the Weibull model no longer fits the data well (Fig. 2a). Consequently, daily wind speed data fail to capture the statistical characteristics or preserve the probability distribution observed in higher resolution data[11].

High-resolution wind speed data better reflect wind speed distributions and offer more accurate WPD assessments. However, these datasets require substantial computational resources and may be more expensive and complicated instruments. Our findings show that 1-hour resolution data strikes an effective balance between accuracy and feasibility (Fig. 2d), aligning with previous studies highlighting the similar statistical characteristics of 10-minute and 1-hour data[11,29]. The widespread availability and reliability of hourly data make it a practical benchmark for WPD calculations.

Crucially, our study demonstrates that the decay of WPD with Δt follows an exponential relationship (Eq. (1)), reflecting the intrinsic properties of wind speed distributions rather than site-specific characteristics. Regions with weaker wind environments, characterized by lower values of parameter a, exhibit higher b values, indicating more rapid WPD decay with coarser Δt (Fig. 2c). This makes underestimation effects particularly pronounced in regions such as East Asia, southern Europe, and eastern USA—areas with relatively flat terrain and extensive wind power deployments[21].

Interestingly, the impact of Δt on WPD is broadly consistent across diverse landscapes (Supplementary Figs. 14, 15, 16), despite variations in surface roughness associated with different land cover types that influence absolute WPD values (Supplementary Note 2). This again underscores that the relationship between WPD and Δt is governed primarily by wind speed distribution characteristics (parameter a), not land surface attributes.

The calibration coefficient, K, is particularly relevant for revisiting earlier WPD assessments that relied on daily or monthly data and likely underestimated wind power potential. Additionally, in scenarios where high-resolution data are unavailable, applying K enables accurate assessments with coarse-resolution datasets, reducing computational costs. Using $K(\Delta t - 1\,\text{hour})$, WPD estimates from commonly used Δt intervals (e.g., 3-hour, 6-hour, daily; Supplementary Table 1) can be harmonized with WPD(1-hour). This calibration approach substantially mitigates underestimations, as demonstrated in Fig. 4f, fostering consistency in wind power assessments across research, industry, and policymaking contexts.

While Δt minimally impacts projected relative changes in future wind speed and WPD, it does affect assessments of primary wind direction (Supplementary Fig. 17), which is critical for turbine alignment and wind farm design (Supplementary Note 3). To improving future wind regime predictions, enhanced simulation capabilities are essential, including better representation of boundary-layer processes, high-resolution models, regional downscaling, and advanced machine learning techniques[30,31]. These advancements will help address uncertainties in wind speed and WPD projections, while accounting for other factors such as air density, complex terrain, surface roughness, and grid resolution[12,32–34]. Ultimately, the proposed calibration method offers a straightforward solution to reduce one prominent source of uncertainty in wind power assessments. By enabling more accurate evaluations, it facilitates effective planning and decision-making in the global transition toward renewable energy.

Methods
Wind datasets
This study utilizes global high temporal-resolution wind speed data, including 20-min, 30-min, and 1-hour observations, sourced from the National Climatic Data Center (NCDC). To ensure data quality and sufficient sample sizes for reliable statistical analyses[10], only stations with >80% valid records spanning 1973–2021 were included in the analysis, as illustrated in Supplementary Fig. 1. Climate reanalysis datasets, such as ERA5, NCEP/NCAR, and NCEP-DOE, were also employed to analyze 10 m and hub-height (100 m) wind speeds[35–37]. Reanalysis datasets are widely recognized for their consistency and high-fidelity in wind speed estimates[38,39]. WPD was calculated across multiple temporal resolutions (e.g., 20-min, 1-hour, 6-hour, daily) for

both observational and reanalysis datasets to quantify the effect of Δt.

For future wind power assessments, this study used outputs from EC-Earth3 model in CMIP6 as a representative example. This model was selected because it provides 3-hour wind speed data, which meets the requirements of this analysis[40]. Previous studies show that EC-Earth3 closely aligns with other CMIP6 models in capturing wind speed trends[41]. Additional CMIP6 models with coarser temporal resolutions (e.g., BCC-CSM2-MR, CMCC-ESM2, CNRM-CM6-1, INM-CM4-8, IPSL-CM6A-LR, MIROC6, MRI-ESM2-0) were used to evaluate relative changes in WPD under future scenarios (Supplementary Fig. 12).

Extrapolating wind speed at hub height
Wind speed at turbine hub height, typically 100 meters above ground level, was extrapolated from 10 m using a stability-corrected logarithmic wind profile[42], as described in Eq. (2)

$$U(z) = \frac{u_*}{\kappa}\left[\ln\left(\frac{z}{z_0}\right) + \Psi\left(\frac{z}{L}\right)\right] \tag{2}$$

where $U(z)$ is the wind speed at height z, u_* is friction velocity, $\kappa = 0.4$ (von Karman constant), z_0 is the surface roughness length, $\Psi(\frac{z}{L})$ is the stability correction term, and L is the Monin-Obukhov length. For neutrally stability conditions[43,44], this equation simplifies to Eq. (3)

$$U(z) = \frac{u_*}{\kappa}\ln\left(\frac{z}{z_0}\right) \tag{3}$$

When height z_1 and z_2 are known, friction velocities cancel out, yielding Eq. (4)

$$\frac{U(z_2)}{U(z_1)} = \frac{\ln(\frac{z_2}{z_0})}{\ln(\frac{z_1}{z_0})} \tag{4}$$

This logarithmic wind profile equation (Eq. (4)) is widely used to extrapolate hub-height wind speed from the observations[20,45–47]. While previous studies often assumed a constant z_0 value, surface roughness varies with land-use and land-cover (LULC)[48]. To improve the accuracy of WPD calculation, this study applied z_0 values specific to LULC types[48–51], as summarized in Supplementary Table 2. LULC types were determined using global land cover data from European Space Agency (ESA) WorldCover[52].

ERA5 provides 100 m wind speed data directly, eliminating the need for extrapolation. These data have been widely used in WPD assessments due to their reliability and consistency[38,46,53]. Furthermore, z_0 was calculated globally using ERA5 wind speed data at 10 m and 100 m, based on Eq. (4)[54,55]. The global z_0 map derived from ERA5 (Supplementary Fig. 18) aligns well with the LULC-specific z_0 values (Supplementary Table 2). This global z_0 map derived from ERA5 was applied to extrapolate hub-height wind speeds in CMIP6 outputs.

Calculation of wind power density and actual electrical power production
WPD, a widely used metric for assessing wind energy potential[4–6], was calculated using the statistical approach described in Eq. (5)

$$WPD = \frac{1}{2n}\sum_{i=1}^{n}\rho U_i^3 \tag{5}$$

where n is the number of observations over a given time period, U_i is the hub-height wind speed (restricted to 3-25 m s^{-1}, corresponding to cut-in and cut-out speeds of wind turbines), and ρ is the air density, assumed to be 1.225 kg m^{-3} (standard value). While air density varies spatially and temporally due to geographic and seasonal factors, a constant p was used here to isolate the effects of Δt on WPD. The

3–25 m s^{-1} range represents the operational limits for most turbines, where wind speeds outside this range contribute no electrical power[14].

To estimate actual electrical power production (AEP), we used the General Electric GE 1.5 s wind turbine as an example[56]. The turbine-specific power curve, shown in Supplementary Fig. 4, includes the following parameters: rated power (1500 kW), cut-in wind speed (3.5 m s^{-1}), rated wind speed (12.0 m s^{-1}), cut-out wind speed (25 m s^{-1}), diameter (70.5 m), swept area (3904.0 m^2), and hub height (100 m). Hourly and daily hub-height wind speed data were applied to this power curve to calculate AEP.

Examination of wind speed probability distribution function
The Weibull probability distribution function (PDF) has been widely used to fit wind speed distributions due to its reliability in capturing observed patterns[23,27,57]. The Weibull PDF is expressed in Eq. (6)

$$f(U) = \frac{k}{c}\left(\frac{U}{c}\right)^{k-1}\exp\left[-\left(\frac{U}{c}\right)^{k}\right] \quad (6)$$

where U is wind speed (m s^{-1}), k is the shape parameter (dimensionless), and c is the scale parameter (m s^{-1}). These parameters can be estimated using methods such as maximum likelihood estimation or least squares fitting[58].

WPD derived from Weibull distributions is calculated using Eq. (7)

$$WPD = \tfrac{1}{2}\rho c^3 \Gamma\left(1+\tfrac{3}{k}\right) \quad (7)$$

where Γ is the gamma function and can be calculated using the method of factorial.

However, our findings reveal substantial discrepancies between WPD estimates derived using the Weibull method and those calculated via the statistical method (Eq. (5)), irrespective of whether hourly or daily data were utilized (Supplementary Figs. 19, 20). These discrepancies are particularly pronounced at low WPD levels (<50 W m^{-2}) or high levels (>400 W m^{-2}) (Supplementary Fig. 20). Previous studies have also highlighted uncertainties in Weibull-based WPD estimates for coarse temporal resolutions[23,29]. Thus, to ensure consistency across different Δt values, we adopted the statistical method (Eq. (5)) for WPD calculations in this study.

Definition and calculation of calibration coefficient K
The relative bias (RB) of WPD calculated from different Δt values, relative to WPD(1-hour), is defined by Eq. (8)

$$RB = \frac{WPD(\Delta t)}{WPD(1 hour)} - 100\% \quad (8)$$

This relationship can be reformulated to express the relationship between WPD(1-hour) and WPD(Δt) as shown in Eq. (9)

$$\frac{WPD(1 hour)}{WPD(\Delta t)} = \frac{1}{RB + 100\%} \quad (9)$$

The calibration coefficient $K(\Delta t - 1\ hour)$, defined as the ratio of WPD(1-hour) to WPD(Δt), is expressed in Eq. (10)

$$K(\Delta t - 1 hour) = \frac{WPD(1 hour)}{WPD(\Delta t)} \quad (10)$$

K values directly correspond to RB (e.g., $K = 5.0$ for RB = -80%; $K = 2.0$ for RB = -50%). WPD(1-hour) was chosen as the target for rectification due to several reasons. First, as shown in Fig. 2d, WPD(1-hour) closely approximates parameter a, which represents the theoretical maximum WPD. This makes it a useful benchmark for wind power assessments. Second, while higher temporal resolution data, such as

10-minute intervals, may offer more precise WPD estimates[29], such data are often unavailable or computationally prohibitive. In contrast, 1-hour resolution data are widely accessible and statistically comparable to 10-minute data[10,59]. Third, practical considerations, such as data availability and computational efficiency, often necessitate the use of even coarser resolutions (e.g., 3-hour, 6-hour, daily, monthly) in WPD calculations (Supplementary Table 1). Using WPD(1-hour) as the standard enables $K(\Delta t - 1\ hour)$ to reliably correct biases introduced by coarse resolutions, ensuring robust adjustments while maintaining computational feasibility.

Data availability
All datasets used in this study are publicly available. High temporal-resolution wind speed observations from NCDC are accessible at https://www.ncei.noaa.gov/maps/hourly/ (last accessed: December 1, 2024). ERA5 reanalysis data are available at https://cds.climate.copernicus.eu/datasets (last accessed: December 1, 2024). NCEP/NCAR and NCEP-DOE reanalysis datasets can be accessed at https://psl.noaa.gov/data/gridded/ (last accessed: December 1, 2024). Wind speed simulation data with 3-hour resolution from EC-Earth3 model are available at the Climate Model Diagnosis and Intercomparison website: https://esgf-node.llnl.gov/projects/cmip6/ (last accessed: December 1, 2024). Global land cover data from ESA WorldCover can be accessed at https://esa-worldcover.org/en (last accessed: December 1, 2024). The calibration coefficient (K) generated in this study are provided in the Supplementary Information and Source Data file. Source data are provided with this paper.

Code availability
The data analysis in this study was performed using Python (version 3.8) with statistical packages. The figures were generated using Python with Cartopy package. All software packages used in this study are publicly accessible.

References
1. Barthelmie, R. J. & Pryor, S. C. Potential contribution of wind energy to climate change mitigation. *Nat. Clim. Chang.* **4**, 684–688 (2014).
2. Lei, Y. et al. Co-benefits of carbon neutrality in enhancing and stabilizing solar and wind energy. *Nat. Clim. Chang.* **13**, 693–700 (2023).
3. Global Wind Energy Council. Global wind report 2024 (GWEC, 2024).
4. Pryor, S. C. & Barthelmie, R. J. Assessing climate change impacts on the near-term stability of the wind energy resource over the United States. *Proc. Natl Acad. Sci. USA.* **108**, 8167–8171 (2011).
5. Tian, Q., Huang, G., Hu, K. & Niyogi, D. Observed and global climate model-based changes in wind power potential over the Northern Hemisphere during 1979–2016. *Energy* **167**, 1224–1235 (2019).
6. Zeng, Z. et al. A reversal in global terrestrial stilling and its implications for wind energy production. *Nat. Clim. Chang.* **9**, 979–985 (2019).
7. Elliott D. L., Holladay C. G., Barchet W. R., Foote H. P. & Sandusky W. F. (1986) *Wind Energy Resource Atlas of the United States* (Solar Technical Information Program, US Department of Energy, Washington, DC), p 210.
8. Pryor, S. C., Nikulin, G. & Jones, C. Influence of spatial resolution on regional climate model derived wind climates. *J. Geophys. Res.* **117**, D03117 (2012).
9. Carvalho, D., Rocha, A., Gómez-Gesteira, M. & Silva Santos, C. WRF wind simulation and wind energy production estimates forced by different reanalyses: Comparison with observed data for Portugal. *Appl. Energy* **117**, 116–126 (2014).
10. Yizhaq, H., Xu, Z. & Ashkenazy, Y. The effect of wind speed averaging time on the calculation of sand drift potential: New scaling laws. *Earth Planet. Sci. Lett.* **544**, 116373 (2020).

11. Effenberger, N., Ludwig, N. & White, R. H. Mind the (spectral) gap: how the temporal resolution of wind data affects multi-decadal wind power forecasts. *Environ. Res. Lett.* **19**, 14015 (2024).

12. Ulazia, A., Sáenz, J., Ibarra-Berastegi, G., González-Rojí, S. J. & Carreno-Madinabeitia, S. Global estimations of wind energy potential considering seasonal air density changes. *Energy* **187**, 115938 (2019).

13. Liang, Y. et al. Estimation of the influences of spatiotemporal variations in air density on wind energy assessment in China based on deep neural network. *Energy* **239**, 122210 (2022).

14. Pryor, S. C. & Barthelmie, R. J. Climate change impacts on wind energy: A review. *Renew. Sustain. Energy Rev.* **14**, 430–437 (2010).

15. Ashkenazy, Y. & Yizhaq, H. The diurnal cycle and temporal trends of surface winds. *Earth Planet. Sci. Lett.* **601**, 117907 (2023).

16. Karnauskas, K. B., Lundquist, J. K. & Zhang, L. Southward shift of the global wind energy resource under high carbon dioxide emissions. *Nat. Geosci.* **11**, 38–43 (2018).

17. Soares, P. M. M., Lima, D. C. A. & Nogueira, M. Global offshore wind energy resources using the new ERA-5 reanalysis. *Environ. Res. Lett.* **15**, 1040a2 (2020).

18. Hosking, J. S. et al. Changes in European wind energy generation potential within a 1.5 °C warmer world. *Environ. Res. Lett.* **13**, 54032 (2018).

19. Miao, H. et al. Evaluation of Northern Hemisphere surface wind speed and wind power density in multiple reanalysis datasets. *Energy* **200**, 117382 (2020).

20. Archer, C. L. & Jacobson, M. Z. Evaluation of global wind power. *J. Geophys. Res.* **110**, D12110 (2005).

21. Lu, X., McElroy, M. B., Kiviluoma, J. & Anderson, J. G. Global Potential for Wind-Generated Electricity. *Proc. Natl Acad. Sci. USA.* **106**, 10933–10938 (2009).

22. Liu, L. et al. Climate change impacts on planned supply–demand match in global wind and solar energy systems. *Nat. Energy* **8**, 870–880 (2023).

23. Pryor, S. C., Nielsen, M., Barthelmie, R. J. & Mann, J. Can satellite sampling of offshore wind speeds realistically represent wind speed distributions? Part II: Quantifying uncertainties associated with distribution fitting methods. *J. Appl. Meteorol.* **43**, 739–750 (2004).

24. Shaw, T. A. et al. Storm track processes and the opposing influences of climate change. *Nat. Geosci.* **9**, 656–664 (2016).

25. Larsén, X. G. & Mann, J. The effects of disjunct sampling and averaging time on maximum mean wind speeds. *J. Wind Eng. Ind. Aerodyn.* **94**, 581–602 (2006).

26. Pryor, S. C. & Barthelmie, R. J. A global assessment of extreme wind speeds for wind energy applications. *Nat. Energy* **6**, 268–276 (2021).

27. Campisi-Pinto, S., Gianchandani, K. & Ashkenazy, Y. Statistical tests for the distribution of surface wind and current speeds across the globe. *Renew. Energy* **149**, 861–876 (2020).

28. Jamil, M., Parsa, S. & Majidi, M. Wind power statistics and an evaluation of wind energy density. *Renew. Energy* **6**, 623–628 (1995).

29. Gil Ruiz, S. A., Barriga, J. E. C. & Martínez, J. A. Wind power assessment in the Caribbean region of Colombia, using ten-minute wind observations and ERA5 data. *Renew. Energy* **172**, 158–176 (2021).

30. Wang, H., Yin, S., Yue, T., Chen, X. & Chen, D. Developing a dynamic-statistical downscaling framework for wind speed prediction for the Beijing 2022 Winter olympics. *Clim. Dyn.* **62**, 7345–7363 (2024).

31. Schmidt, L. & Ludwig, N. Wind power assessment based on super-resolution and downscaling - a comparison of deep learning methods. *arXiv*:2407.08259. https://doi.org/10.48550/arXiv.2407.08259 (2024).

32. Jung, C. & Schindler, D. A review of recent studies on wind resource projections under climate change. *Renew. Sustain. Energy Rev.* **165**, 112596 (2022).

33. Minola, L. et al. Climatology of near-surface wind speed from observational, reanalysis and high-resolution regional climate model data over the Tibetan Plateau. *Clim. Dyn.* **62**, 933–953 (2024).

34. Deng, X. et al. Offshore wind power in China: A potential solution to electricity transformation and carbon neutrality. *Fundam. Res.* **4**, 1206–1215 (2024).

35. Kalnay, E. et al. The NCEP/NCAR 40-Year Reanalysis Project. *Bull. Am. Meteorol. Soc.* **77**, 437–472 (1996).

36. Kanamitsu, M. et al. NCEP-DOE AMIP-II Reanalysis (R-2). *Bull. Amer. Meteorol. Soc.*, 1631-1643 (2002).

37. Hersbach, H. et al. The ERA5 global reanalysis. *Q. J. R. Meteorol. Soc.* **146**, 1999–2049 (2020).

38. Olauson, J. E. R. A. 5 The new champion of wind power modelling? *Renew. Energy* **126**, 322–331 (2018).

39. Kalverla, P. C., Holtslag, A. A. M., Ronda, R. J. & Steeneveld, G. J. Quality of wind characteristics in recent wind atlases over the North Sea. *Q. J. R. Meteorol. Soc.* **146**, 1498–1515 (2020).

40. Eyring, V. et al. Overview of the Coupled Model Intercomparison Project Phase 6 (CMIP6) experimental design and organization. *Geosci. Model Dev.* **9**, 1937–1958 (2016).

41. Gunn, A., East, A. & Jerolmack, D. J. 21st-century stagnation in unvegetated sand-sea activity. *Nat. Commun.* **13**, 3670 (2022).

42. Stull, R. B. *An Introduction to Boundary Layer Meteorology* (Springer, 1988).

43. Irwin, J. S. A theoretical variation of the wind profile power-law exponent as a function of surface roughness and stability. *Atmos. Environ.* **13**, 191–194 (1979).

44. Emeis, S. Vertical wind profiles over an urban area. *Meteorol. Z.* **13**, 353–359 (2004).

45. Justus, C. G. & Mikhail, A. Height variation of wind speed and wind distributions statistics. *Geophys. Res. Lett.* **3**, 261–264 (1976).

46. Pryor, S. C., Barthelmie, R. J., Bukovsky, M. S., Leung, L. R. & Sakaguchi, K. Climate change impacts on wind power generation. *Nat. Rev. Earth Environ.* **1**, 627–643 (2020).

47. Tong, D. et al. Geophysical constraints on the reliability of solar and wind power worldwide. *Nat. Commun.* **12**, 6146 (2021).

48. Manwell, J. F., McGowan, J. G. & Rogers, A. L. *Wind Energy Explained: Theory, Design and Application* (Wiley, 2010).

49. Emeis, S. Vertical variation of frequency distributions of wind speed in and above the surface layer observed by sodar. *Meteorol. Z.* **10**, 141–149 (2001).

50. Masters, G. M. *Renewable and Efficient Electric Power Systems* (Wiley, 2004).

51. Bañuelos-Ruedas, F., Angeles-Camacho, C. & Rios-Marcuello, S. Analysis and validation of the methodology used in the extrapolation of wind speed data at different heights. *Renew. Sustain. Energy Rev.* **14**, 2383–2391 (2010).

52. Zanaga, D. et al. ESA WorldCover 10 m 2021 v200. https://doi.org/10.5281/zenodo.7254221 (2022).

53. Costoya, X., DeCastro, M., Carvalho, D., Feng, Z. & Gómez-Gesteira, M. Climate change impacts on the future offshore wind energy resource in China. *Renew. Energy* **175**, 731–747 (2021).

54. Carvalho, D., Rocha, A., Costoya, X., DeCastro, M. & Gómez-Gesteira, M. Wind energy resource over Europe under CMIP6 future climate projections: What changes from CMIP5 to CMIP6. *Renew. Sustain. Energy Rev.* **151**, 111594 (2021).

55. Jung, C. & Schindler, D. The role of the power law exponent in wind energy assessment: A global analysis. *Int. J. Energy Res.* **45**, 8484–8496 (2021).

56. Wind-turbine-models.com. *The wind turbine GE 1.5s*. https://www.en.wind-turbine-models.com/turbines/565-ge-vernova-ge–1.5s (2024). (last accessed: December 1, 2024).
57. Pavia, E. G. & O'Brien, J. J. Weibull statistics of wind speed over the ocean. *J. Appl. Meteorol.* **25**, 1324–1332 (1986).
58. Justus, C. G., Hargraves, W. R., Mikhail, A. & Graber, D. Methods for estimating wind speed frequency distributions. *J. Appl. Meteorol.* **17**, 350–353 (1978).
59. Sherman, P., Chen, X. & McElroy, M. B. Wind-generated Electricity in China: Decreasing potential, inter-annual variability and association with changing climate. *Sci. Rep.* **7**, 16294 (2017).

Author contributions
Z.X. designed the research. C.H. performed the analysis. C.H., Z.X. and K.B.K. wrote the draft. C.H., Z.X., K.B.K., D.H. and H.L. contributed to the interpretation of the results and the writing of the paper.

Competing interests
The authors declare no competing interests.

Additional information
Supplementary information The online version contains supplementary material available at https://doi.org/10.1038/s41467-025-59195-2.

Correspondence and requests for materials should be addressed to Zhiwei Xu.

Peer review information *Nature Communications* thanks Christopher Jung, Russell McKenna who co-reviewed with Ruihong Chen, and the other, anonymous, reviewers for their contribution to the peer review of this work. A peer review file is available.

Reprints and permissions information is available at http://www.nature.com/reprints

Publisher's note Springer Nature remains neutral with regard to jurisdictional claims in published maps and institutional affiliations.